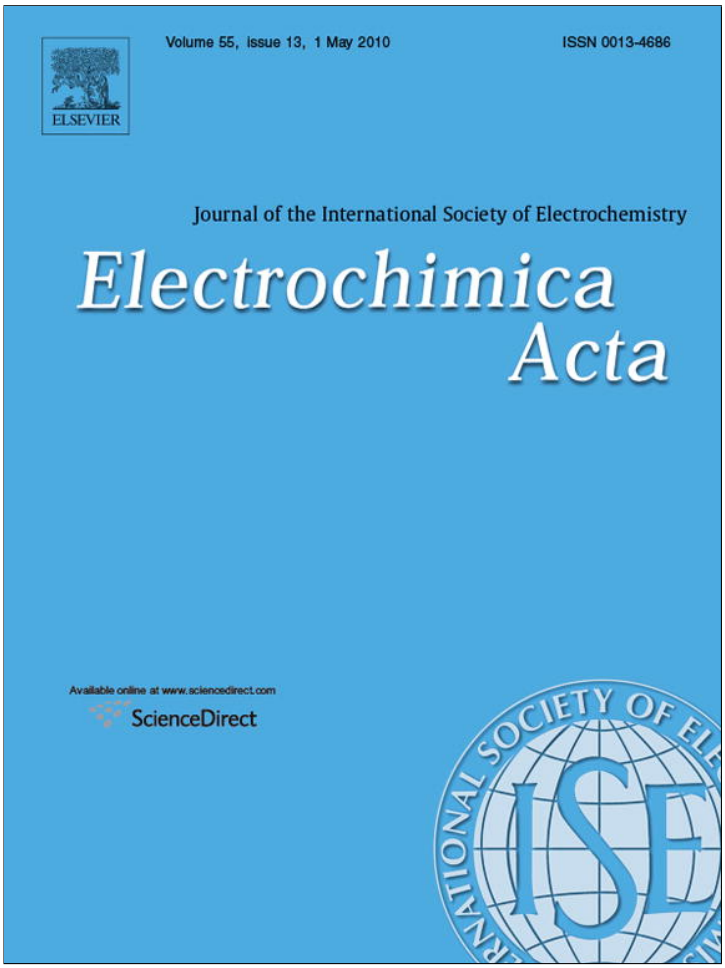

Electrochimica Acta 55 (2010) 4124–4129

Contents lists available at ScienceDirect

Electrochimica Acta

journal homepage: www.elsevier.com/locate/electacta

Electrochemical study of the interaction between Eu^{3+} and ciliate *Euplotes octocarinatus* centrin

Baojuan Zhou, Ziwei Wang, Yanni Tian*, Zhijun Wang, Binsheng Yang*

Institute of Molecular Science, Key Laboratory of Chemical Biology and Molecular Engineering of Ministry of Education, Shanxi University, Taiyuan 030006, PR China

ARTICLE INFO

Article history:
Received 6 October 2009
Received in revised form 23 February 2010
Accepted 26 February 2010
Available online 4 March 2010

Keywords:
Ciliate *Euplotes octocarinatus* centrin
P_{23}
Eu^{3+}
Electrochemical parameters
Binding affinity

ABSTRACT

A new species was formed when protein P_{23} (one segment of ciliate *Euplotes octocarinatus* centrin) was added to a solution of Eu^{3+}. The interaction between P_{23} and Eu^{3+} was investigated by cyclic voltammetry, pulse voltammetry and electrochemical impedance spectroscopy in 10 mM *N*-2-hydroxyethylpiperazine-*N*-2-ethanesulfonic acid (HEPES) buffer (pH 7.4) using a pyrolytic graphite electrode. The formal potential ($E^{o\prime}$) of Eu^{3+} shifted from −0.61 to −0.84 V (versus saturated calomel electrode) after P_{23} was added to the Eu^{3+} solution. The diffusion coefficient (D), the charge-transfer coefficient (α) and the electron transfer standard rate constant (k_s) were obtained in the absence and the presence of P_{23}. The affinity constant of Eu^{3+} and P_{23} was determined to be $(1.89 \pm 0.51) \times 10^4\ M^{-1}$. The electrochemical investigation of europium bound to the protein provided useful data for the studies of calcium-binding proteins.

1. Introduction

Ciliate *Euplotes octocarinatus* centrin (EoCen) [1], composed of 168 amino acids, is a low molecular mass protein (20 kDa) that belongs to EF-hand calmodulin (CaM). The protein contains four helix–loop–helix domains with two high affinity sites for Ca^{2+} in the C-terminal and two low affinity sites in N-terminal [2,3].

Unlike some transition metal ions, Ca^{2+} has a closed electronic shell and therefore lacks electronic, magnetic and spectroscopic properties. This spectroscopic silence can be a disadvantage in studies of the macromolecular environment of calcium. According to Williams [4], lanthanide ions could serve as probes for calcium active sites of protein. The trivalent lanthanide ions, by virtue of the multitude of their spectroscopic and magnetic properties, have been considered suitable as probes of macromolecular environment and structure [5,6].

Lanthanides have been applied to different fields of biomolecules due to their unique luminescent properties [7–9]. Early studies often determined an interdomain distance using luminescence of bound lanthanide ions [10,11]. The solution structures of proteins were subsequently solved by nuclear magnetic resonance (NMR) employing paramagnetic relaxation enhancements and pseudocontact shifts of the Ga^{3+} [12], Ce^{3+} [13] and Tb^{3+} ions [14]. Furthermore, proteins were crystallized with Ho^{3+} [15] and Eu^{3+} [16]. Circularly polarized luminescence from Tb^{3+}, used as a probe for the metal ions in calcium-binding proteins, was studied by Coruh and Riehl [17]. The use of trivalent lanthanide ions as replaceable metal ion in calcium-binding proteins is well established [18,19]. Laser-induced luminescence studies of Eu^{3+} in the EF-hand sites of Ca^{2+}-binding proteins has provided insight into the binding behavior of metal ions [20–25].

In order to obtain more information of the affinity sites in EoCen we prepared a truncated ciliate EoCen, P_{23}, including the second EF-hand domain in the N-terminal and the third EF-hand domain in C-terminal domains by using biological engineering method [1]. Furthermore, based on the result from coordination of EoCen to Tb^{3+} ions [2], we carried out a detailed survey of Eu^{3+} binding in the affinity sites of P_{23} using electrochemistry.

2. Experimental

2.1. Apparatus and reagents

All electrochemical measurements were carried out using a CHI 660B electrochemistry workstation (Shanghai CH Instruments, China) and the impedance data were fit by the EvolCRT software. Circular dichroism (CD) spectra were recorded in the wavelength range of 200–250 nm in a 0.2-cm path length cuvette on a BioLogic MOS 450 spectrometer at room temperature.

The electrochemical cell (volume approximately 800–1000 μL) was a standard two-compartment glass cell with a conventional three-electrode configuration. The side-arm contained the reference electrode, and a saturated calomel electrode (SCE) was connected to the working compartment via a Luggin capillary. The

* Corresponding authors. Tel.: +86 351 7010699; fax: +86 351 7016358.
E-mail addresses: tianyann@sxu.edu.cn (Y. Tian), yangbs@sxu.edu.cn (B. Yang).

0013-4686/$ – see front matter © 2010 Elsevier Ltd. All rights reserved.
doi:10.1016/j.electacta.2010.02.084

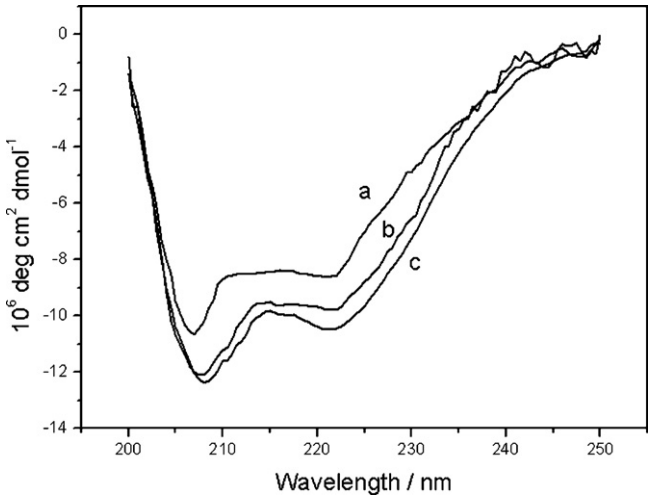

Fig. 1. Circular dichroism spectra of (a) P_{23}, (b) 2:1 concentration ratio of Ca^{2+} and P_{23}, (c) 2:1 concentration ratio of Eu^{3+} and P_{23}, in 10 mM pH 7.4 HEPES buffer ($C_{P_{23}}$: 4.64×10^{-5} M).

edge-plane pyrolytic graphite (PG) working electrodes were constructed from pyrolytic graphite (Advanced Ceramics Corp.), cut perpendicular to the *a*–*b* plane and housed in teflon sheaths. Prior to each experiment, the PG electrodes were cleaned by polishing with an alumina–water slurry (high-purity Al_2O_3, particle size 0.3 and 0.05 μm, BDH) and sonicated briefly, followed by thorough rinsing with water. The surface area of electrodes was calculated according to the Randle–Sevcik equation and the diffusion coefficient of $K_3Fe(CN)_6$. The counter-electrode was a piece of platinum gauze. The working solution was purged with oxygen-free nitrogen for at least 10 min prior to experiments and a nitrogen environment was maintained over the solution in the cell.

N-2-hydroxyethylpiperazine-*N*-2-ethanesulfonic acid (HEPES) was purchased from Sigma and used without further purification. All other chemicals were of analytical grade. All solutions were prepared in doubly distilled water. The Eu^{3+} stock solution was prepared by dissolving the appropriate mass of Eu_2O_3 in hydrochloric acid, which was then standardized with EDTA using xylenol orange as indicator in 0.1 M HAc–NaAc buffer at pH 5.5

2.2. Protein expression and purification

A truncated ciliate EoCen, P_{23}, including the second and the third EF-hand domain, was obtained using biological engineering methods. Recombinant P_{23} was expressed and purified as described by He et al. [1] and Wang et al. [26]. The protein concentration was measured spectrophotometrically at 280 nm using molar extinction coefficients of 2800 M^{-1} cm^{-1} for P_{23}. The extinction coefficient of P_{23} was estimated from the Tyr and Trp content as described by Pace et al. [27].

3. Results and discussion

3.1. Analysis of conformational changes of P_{23} in the presence of Eu^{3+} from circular dichroism spectroscopy

The circular dichroism spectrum of P_{23} is shown in Fig. 1a. Two minima at 208 and 222 nm are observed, which are typical of a protein rich in α-helix domains. An increase in molar ellipticity (222 nm) is observed in the presence of Ca^{2+} (Fig. 1b) and Eu^{3+} (Fig. 1c). Binding of either Ca^{2+} or Eu^{3+} induces secondary structure changes characterized by an increase in α-helix content. Minimal differences in the spectra between the two metal complexes indicate the structural similarity between the two complexes [28].

3.2. Voltammetric behavior of Eu^{3+} in the absence and presence of P_{23} at PG electrodes

Fig. 2 shows the cyclic voltammogram of Eu^{3+} in 0.01 M HEPES buffer (pH 7.4) containing 0.1 M KCl supporting electrolyte at a bare PG electrode (curve a). A pair of well-defined redox peaks appeared at −0.57 V(E_{pa}) and −0.65 V(E_{pc}). The peak separation (ΔE_p), 84 mV, indicated a quasireversible single-electron redox process. The formal potential, $E_b^{0'}$ (or voltammetric $E_{1/2}$) of −0.61 V was estimated from the average of E_{pc} and E_{pa}. In addition, a linear relationship between the peak current and the square root of the scan rate (not shown here) was observed and suggested that the electrode reaction of Eu^{3+} was a diffused-controlled electrode process.

Next, the cyclic voltammograms of Eu^{3+} in the presence of P_{23} in pH 7.4 HEPES buffer are shown as curves b–e in Fig. 2. The addition of P_{23} made the original peak currents decrease gradually and a new pair of redox peaks appeared. Finally, when the concentration of P_{23} was added to half concentration of Eu^{3+}, the original peak current disappeared completely and a pair of well-defined redox peaks appeared at −0.81 V(E_{pa}) and −0.87 V(E_{pc}) (Fig. 2e), with a peak potential separation (ΔE_p) of 66 mV. The formal potential ($E_b^{0'}$) was −0.84 V and the negative shift of potential was 0.23 V.

There are some similarities between the differential pulse voltammetry (DPV) and cyclic voltammetry. As shown in Fig. 3, as the concentration of P_{23} was increased from 0 to 9.1×10^{-5} M (half concentration of Eu^{3+}), the original peak current of Eu^{3+} at −0.59 V gradually decreased in magnitude, while a new peak at −0.80 V gradually increased. After the concentration of P_{23} was increased up to above 9.1×10^{-5} M, the former peak disappeared completely and the latter peak no longer increased. A negative potential shift of 0.21 V was observed, which was consistent with the potential shift shown in Fig. 2. The current peak at −0.84 V in the CV and −0.80 V in DPV most likely arose when Eu^{3+} enters the Ca^{2+}-binding sites of P_{23} to form a new complex.

It should be noted that there are two binding sites in each P_{23} that each allow for binding of an Eu^{3+} ion. When Eu^{3+} complexes with P_{23}, however, only a pair of redox peaks was observed in the CV and DPV. We assume an equal binding affinity between Eu^{3+} and each of the two binding sites of P_{23}. In this work, $P_{23}^{@}$ was used

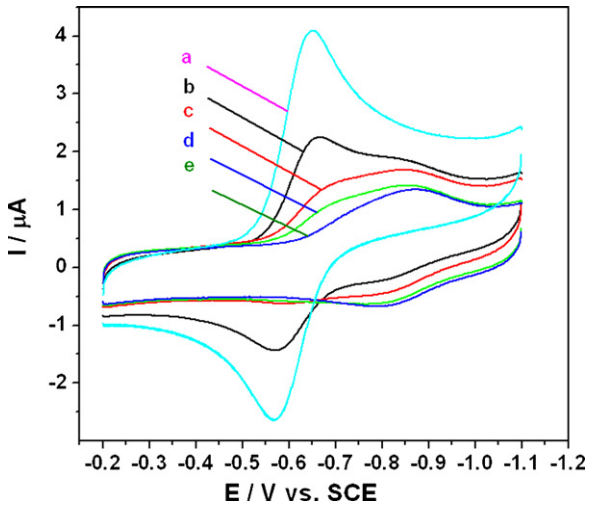

Fig. 2. Cyclic voltammograms of the different concentration ratios of Eu^{3+} and P_{23} (a) 10:0; (b) 10:1; (c) 10:2; (d) 10:3; (e) 10:5; after mixed 30 min at scan rate of 100 mV/s, in 10 mM pH 7.4 HEPES buffer ($C_{Eu^{3+}}$: 1.82×10^{-4} M).

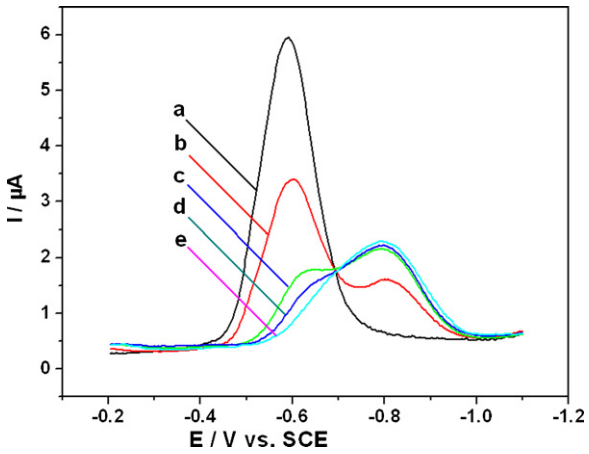

Fig. 3. DPV of the different concentration ratios of Eu^{3+} and P_{23} (a) 10:0; (b) 10:1; (c) 10:2; (d) 10:3; (e) 10:5; after mixed 30 min at scan rate of 100 mV/s, in 10 mM pH 7.4 HEPES buffer ($C_{Eu^{3+}}$: 1.82×10^{-4} M).

to express a half-P_{23} with only one binding site. Therefore, with a 2:1 concentration ratio between Eu^{3+} and P_{23} a 1:1 concentration ratio between Eu^{3+} and $P_{23}^{@}$ was expected.

When the concentration ratio of Eu^{3+} and $P_{23}^{@}$ was 1:1, CVs were performed in 10 mM HEPES buffer (pH 7.4) at various scan rates as shown in Fig. 4A. The scan rate dependence experiments revealed that the peak current increase linearly with the square root of the potential scan rate at scan rates from 0.10 to 0.72 V s^{-1} (Fig. 4B), indicating a diffused-controlled electrode process. Fig. 4C is the plot of E_p versus ln ν, which is used later for the calculation.

3.3. Comparison of the electrochemical parameters in the absence and the presence of P_{23}

3.3.1. EIS response

In electrochemical impedance spectroscopy (EIS), the semicircle feature at higher frequencies corresponds to an electron transfer limited process. As shown in Fig. 5, the semicircle is changed

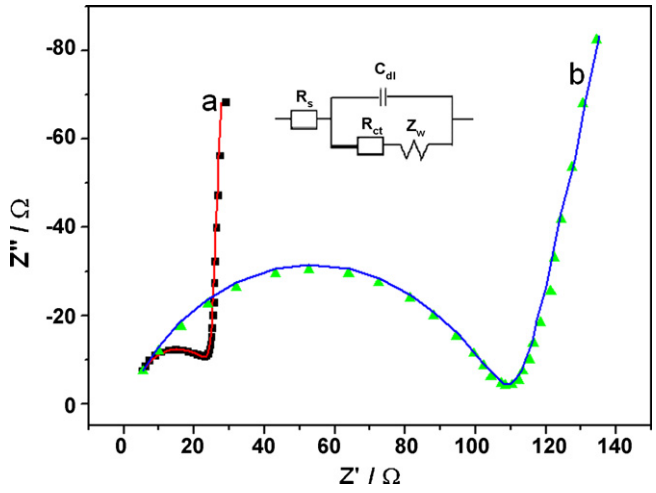

Fig. 5. EIS of the different concentration ratios of Eu^{3+} and $P_{23}^{@}$ (a) 1:0; the frequency range is in 0.1–10^5 Hz at 0.61 V; (b) 1:1; the frequency range is in 0.1–10^5 Hz at 0.84 V; in 10 mM pH 7.4 HEPES buffer containing 0.1 M KCl, ($C_{Eu^{3+}}$: 1.90×10^{-4} M). The inset shows the equivalent circuit used to model impedance data.

Table 1
Values of each element in the equivalent circuit for different concentration ratios of Eu^{3+} ($C_{Eu^{3+}}$: 1.90×10^{-4} M) and $P_{23}^{@}$.

Concentration ratio of Eu^{3+} and $P_{23}^{@}$	R_s/Ω cm^2	R_{et}/Ω cm^2	C_{dl}/μF cm^2
1:0	2.81	24.37	0.197
1:1	0.423	117.7	0.0419

when Eu^{3+} complexes with P_{23}. The equivalent circuit for an electrode–solution interface undergoing heterogeneous electron transfer is usually modeled by Randle's equivalent circuit as shown in the inset of Fig. 5.

Electrolyte resistance (R_s), double layer capacitance (C_{dl}) and electron transfer resistance (R_{et}) were calculated based on an equivalent circuit to fit the experimental impedance result in Fig. 5. Impedance data are shown in Table 1.

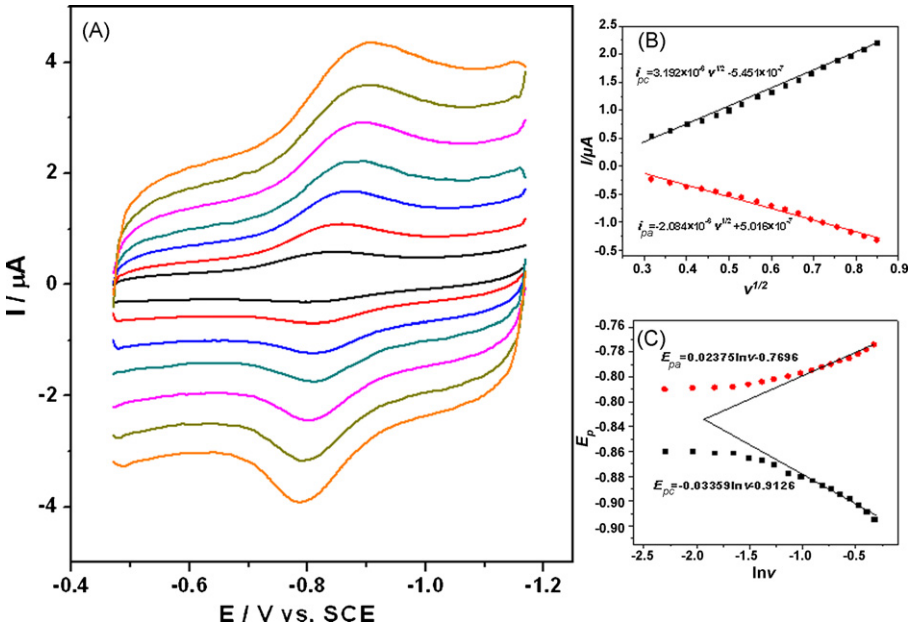

Fig. 4. (A) Cyclic voltammograms of Eu^{3+} and $P_{23}^{@}$ (1:1 concentration ratio, $C_{Eu^{3+}}$: 1.82×10^{-4} M) in 10 mM pH 7.4 HEPES buffer at various scan rates 30, 70, 130, 190, 270, 350 and 430 mV/s, respectively. (B) The dependence of cathodic and anodic peak current on the square root of scan rate. (C) Plot of cathodic and anodic peak potential versus ln ν.

As expected, the calculated results show that R_{et} of the solution increased after the complex of Eu^{3+} and P_{23} formed. The macromolecular compound introduced a barrier to the interfacial electron transfer.

3.3.2. The diffusion coefficient (D), electron transfer coefficient (α) and electron transfer rate constant (k_s)

The kinetic parameters of Eu^{3+} and the complex of Eu^{3+} and P_{23} at the PG electrode could be obtained. First, the diffusion coefficient (D) can be calculated according to the Rardles–Sevcik equation [29]:

$$i_p = 2.69 \times 10^5 A n^{3/2} D^{1/2} C v^{1/2}$$

where A denotes the area of the electrode, n denotes the number of electrons transferred and C is the concentration. Based on known values of A, n and C, the slope of i_p versus $v^{1/2}$ plot will yield an estimate for D. In this work, by constructing an i_p versus $v^{1/2}$ plot based on the current peak, we obtained diffusion constants of 6.26×10^{-6} cm^2 s^{-1} for Eu^{3+} and 1.27×10^{-6} cm^2 s^{-1} for the complex of Eu^{3+} with P_{23}.

The electron transfer coefficient (α) and electron transfer rate constant (k_s) can be obtained according to the following equations [30]:

$$E_p = E^0 + \frac{RT}{-\alpha nF}[0.780 + \ln(Db)^{1/2} - \ln k_s], \quad b = \frac{\alpha nF v}{RT}$$

$$i_p = 0.227 nFAC_0 k_s \times \exp\left[\frac{-\alpha nF}{RT}(E_p - E^0)\right]$$

From the slope of E_p versus $\ln v$ (Fig. 4C) and the intercepts of $\ln i_p$ versus $\ln v$, α and k_s of Eu^{3+} are 0.62 and 3.41×10^{-2} s^{-1}, and α and k_s of the complex of Eu^{3+} with P_{23} are 0.47 and 1.13×10^{-2} s^{-1}, respectively.

The facts mentioned above, the obtained electron transfer resistance (R_{et}) in EIS experiments, the calculated electron transfer coefficient (α) and the electron transfer rate constant (k_s) imply that the kinetic process of electron transfer was slow for the Eu^{3+}–P_{23} system. Usually, rare earth ions can bind to the oxygen of an amide group in the peptide chain of the protein and enzyme to form a complex of the rare earth ion and the protein or enzyme molecule [31]. When Eu^{3+} interacts with P_{23}, it may form a complex. The resultant complex is a large molecule and its electron transfer must be more difficult than that of Eu^{3+}. Thus, the electron transfer coefficient and the electron transfer rate constant of the complex should be smaller than that of Eu^{3+}. The current density of the complex is smaller than that of Eu^{3+}. In addition, the electrochemical reaction of Eu^{3+} would relate to the microenvironment. After forming the complex, the microenvironment of Eu^{3+} is changed. Thus, the redox potential is changed.

3.4. Analyses of the binding between Eu^{3+} and P_{23}

Based on a conventional square mechanism [32] the net shift in $E_{1/2}$ can be used to estimate the ratio of equilibrium constants for P_{23} binding to Eu^{3+} or Eu^{2+} ions.

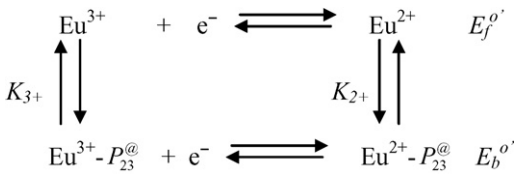

Here, $E_f^{o'}$ and $E_b^{o'}$ are the formal potentials of the Eu^{3+}/Eu^{2+} couple and Eu^{3+}–$P_{23}^{@}$/Eu^{2+}–$P_{23}^{@}$ couple, respectively. Based on the Nernst equations for reversible redox reactions of each species and the corresponding equilibrium constants of $P_{23}^{@}$ binding to each oxidation state, the single-electron redox process is:

$$E_b^{o'} - E_f^{o'} = 0.059 \log\left(\frac{K_{2+}}{K_{3+}}\right)$$

Thus, for a limiting shift of −0.23 V, K_{2+}/K_{3+} is 1.31×10^{-4}, meaning that Eu^{2+}–$P_{23}^{@}$ is less stable than Eu^{3+}–$P_{23}^{@}$. In other words, the Eu^{3+} ion is bound more strongly than the Eu^{2+} ion. Some complexes of the Eu^{2+} reported by Merbach [33] were more easily oxidized than the octaaqua ion $[Eu(H_2O)_8]^{2+}$. This may be explained by the greater number carboxylate groups that bind Eu^{3+} and stabilize the Eu^{3+} complexes. As reported in the literature [34–37], all known EF-hand crystal structures display a pentagonal bipyramidyl coordination geometry in which the Ca^{2+} ion is coordinated to seven oxygen ligands from the side chains of residues 1, 3, 5, and 12, the main chain carbonyl of position 7, as well as a bridged water at position 9 [38]. Horrocks used a luminescence spectroscopy to determine the number of water molecules coordinated to Eu^{3+} and Tb^{3+} in proteins [23,39] and suggested that lanthanide ions generally had one more coordination number than Ca^{2+} in well-formed protein sites. Therefore, lanthanide ions are often ligated by an additional water molecule [39]. The coordination number of the lanthanide ion is possibly higher than that of Ca^{2+} in the same site. Ca^{2+} ions may be replaced by Eu^{3+} ions due to the nearly identical ionic radii of these ions (7-coordinate Ca^{2+} 1.20 Å; 8-coordinate Eu^{3+} 1.21 Å) [24]. In addition to the 7 oxygen ligands including carboxylate groups in P_{23}, another oxygen atom of water molecule may coordinate to Eu^{3+}.

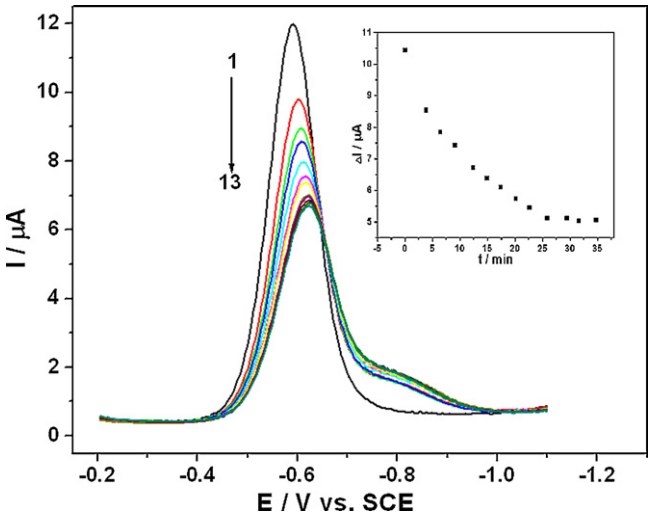

Fig. 6. The variety of the DPV curves with the reaction time when the concentration ratio of Eu^{3+} and $P_{23}^{@}$ is 8:1, ($C_{Eu^{3+}}$: 3.24×10^{-4} M). Inset: plot of peak current versus reaction time.

3.5. Kinetic analysis for the affinity of P_{23} binding to Eu^{3+}

According to the method of Minunni et al. [40] and Hock and He et al. [41], DPV was employed to calculate the affinity constant of Eu^{3+} and P_{23}. Fig. 6 shows the DPV curves obtained after a 30-min reaction between P_{23} and Eu^{3+} at 25 °C. The process was carried out five times using different concentrations of Eu^{3+} and P_{23} to obtain the data in Table 2. Here, the Δi of the current at −0.80 V was directly attributed to the mass of Eu^{3+}–$P_{23}^{@}$.

For the kinetic process of the reversible interaction $Eu^{3+} + P_{23}^{@} \rightleftharpoons Eu^{3+} - P_{23}^{@}$ the formation rate of the product at time t may be written as:

$$\frac{d[Eu^{3+} - P_{23}^{@}]}{dt} = k_{ass} \times [Eu^{3+}] \times [P_{23}^{@}] - k_{diss} \times [Eu^{3+} - P_{23}^{@}] \quad (1)$$

Table 2
Data handing results of $d[\Delta i]/dt$ versus Δi and the values of correlation coefficient.

Eu^{3+} concentration	Linear regression equation	r	$-SL\ (min^{-1})$
1.62×10^{-4} M	$-d(\Delta i)/dt = -1.75\times10^{-7} + 0.0371\Delta i$	0.9899	0.0371
2.43×10^{-4} M	$-d(\Delta i)/dt = -3.76\times10^{-7} + 0.0543\Delta i$	0.9765	0.0543
3.24×10^{-4} M	$-d(\Delta i)/dt = -6.51\times10^{-7} + 0.0842\Delta i$	0.9865	0.0842
4.04×10^{-4} M	$-d(\Delta i)/dt = -7.64\times10^{-7} + 0.102\Delta i$	0.9884	0.102
4.86×10^{-4} M	$-d(\Delta i)/dt = -1.03\times10^{-6} + 0.137\Delta i$	0.9869	0.137

where k_{ass} is the association rate constant and k_{diss} is the dissociation rate constant.

Since Δi of the current was proportional to the mass of Eu^{3+}–$P_{23}^{@}$, Δi_m was attributed to the complete reaction of $P_{23}^{@}$ with Eu^{3+}. Therefore, the concentration of free $P_{23}^{@}$ was directly proportional to $(\Delta i_m - \Delta i)$. Eq. (1) can thus be expressed as:

$$\frac{d[\Delta i]}{dt} = k_{ass} \times [Eu^{3+}] \times [\Delta i_m - \Delta i] - k_{diss} \times [\Delta i] \quad (2)$$

and transformed to:

$$\frac{d[\Delta i]}{dt} = -(k_{ass} \times [Eu^{3+}] + k_{diss})\Delta i + k_{ass} \times \Delta i_m \times [Eu^{3+}] \quad (3)$$

The slope SL can be obtained as follows:

$$SL = (k_{ass} \times [Eu^{3+}] + k_{diss}) \quad (4)$$

where $[Eu^{3+}]$ is the concentration of free Eu^{3+}. When $C_{Eu^{3+}}$ is far more than $C_{P_{23}}$ $[Eu^{3+}]$ is the initial concentration in a mass of solution.

Based on Eq. (4) and the experimental data in Table 2 [42], the SL value was plotted against the concentration of Eu^{3+}, as shown in Fig. 7. The linear regression equation for the DPV method was $-SL = 3.06\times10^{2}C + 0.0162$ (SL: min^{-1}, C: M) with a correlation coefficient of 0.995 at 25 °C. Therefore, k_{ass} and k_{diss} could be calculated from the slope and intercept of the linear fit, and were found to be:

$$k_{ass} = 3.06\times10^{2}\ M^{-1}\ min^{-1}$$

$$k_{diss} = 0.0162\ min^{-1}$$

The affinity constant K for $Eu^{3+} - P_{23}^{@}$ can be obtained as a ratio:

$$K = \frac{k_{ass}}{k_{diss}} = (1.89 \pm 0.51)\times10^{4}\ M^{-1}$$

In comparison with a spectroscopic method based on fluorescence titration curves, the conditional affinity constant of the Tb^{3+}–P_{12} system was determined to be $(2.13 \pm 0.10)\times10^{5}\ M^{-1}$ [2]. The difference in the conditional affinity constant may arise from two general factors. One factor is the different electrostatic interactions between Eu^{3+} and Tb^{3+}. When the electric charge is the same, the slightly larger ionic radius of Eu^{3+} may weaken the binding in P_{23}. The other factor is due to the influence of different experimental methods. For example, in spectroscopic methods, viscosity does not have a prominent effect, but in electrochemical methods, it affects the mass transference and diffusion. Therefore, the data for interaction between Eu^{3+} and P_{23} obtained by electrochemistry is reliable.

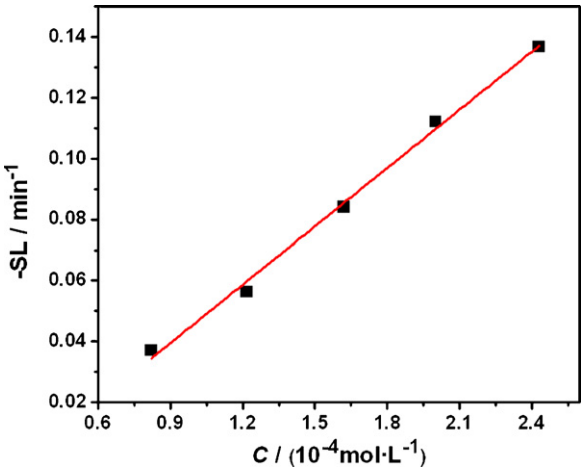

Fig. 7. Dependence of −SL on the concentration of Eu^{3+} at 25 °C.

4. Conclusion

In this paper, we studied the electrochemical behavior of the interaction between Eu^{3+} and P_{23}. The current peak at −0.84 V in the CV of the Eu^{3+}–P_{23} system was different that observed for Eu^{3+} at −0.61 V. This change indicated that a reaction occurred between Eu^{3+} and P_{23} and suggested that Eu^{3+} ions entered into the Ca^{2+}-binding sites of P_{23} to form a new $Eu_2{}^{3+}$–P_{23} complex.

Acknowledgements

This project is supported by the Natural Science Foundation of PRC China (No. 20771068 and No. 20901048) and the Natural Science Foundation of Shanxi Province (No. 2006011016).

References

[1] X.J. He, J.Y. Feng, W. Wang, B.F. Chai, B.S. Yang, A.H. Liang, Acta Zool. Sinica 50 (2004) 445.
[2] L.X. Ren, Y.Q. Zhao, J.Y. Feng, X.J. He, A.H. Liang, B.S. Yang, Chin. J. Inorg. Chem. 22 (2006) 87.
[3] N.D. Moncrief, R.H. Kretsincer, M. Goodman, Mol. Evol. 30 (1990) 522.
[4] R.J.P. Williams, Tilden Lecture. Quart. Rev. Chem. Soc. London 24 (1970) 331.
[5] R.A. Dwek, R.E. Richards, Eur. J. Biochem. 21 (1971) 204.
[6] J. Reuben, Die Naturwissenschaften 62 (1975) 172.
[7] W.D. Horrocks Jr., R.S. Daniel, J. Am. Chem. Soc. 101 (1979) 334.
[8] W.D. Horrocks Jr., D.R. Sudnick, Science (Washington, DC) 206 (1979) 1194.
[9] I. Hemmilä, V. Laitala, J. Fluoresc. 15 (2005) 529.
[10] W.D. Horrocks Jr., B. Holmquist, B.L. Vallee, Proc. Natl. Acad. Sci. U.S.A. 72 (1975) 4764.
[11] W.J. Dong, J.M. Robinson, J. Xing, P.K. Umeda, H.C. Cheung, Protein Sci. 9 (2000) 280.
[12] J.L. Dimicoli, J. Bieth, Biochemistry 16 (1977) 5532.
[13] D. Bentrop, I. Bertini, M.A. Cremonini, S. Forsén, C. Luchinat, C. Luchinat, A. Malmendal, Biochemistry 36 (1997) 11605.
[14] R.R. Biekofsky, F.W. Muskett, J.M. Schmidt, S.R. Martin, J.P. Browne, P.M. Bayley, J. Feeney, FEBS Lett. 460 (1999) 519.
[15] D.E. Brodersen, M. Etzerodt, P. Madsen, J.E. Celis, H.C. Thøgersen, J. Nyborg, M. Kjeldgaard, Structure 6 (1998) 477.
[16] B.W. Matthews, L.H. Weaver, Biochemistry 13 (1974) 1719.
[17] N. Coruht, J.P. Riehl, Biochemistry 31 (1992) 7970.
[18] E. Nieboer, Struct. Bond. (Berlin) 22 (1975) 1.
[19] K.J. Ellis, Znorg. Perspect. Biol. Med. 1 (1977) 101.
[20] M.-J. Rhee, D.R. Sudnick, V.K. Arkle, W.D. Horrocks Jr., Biochemistry 20 (1981) 3328.
[21] A.P. Snyder, D.R. Sudnick, V.K. Arkle, W.D. Horrocks Jr., Biochemistry 20 (1981) 3334.
[22] M.-J. Rhee, W.D. Horrocks Jr., D.P. Kosow, Biochemistry 21 (1982) 4524.
[23] J. Bruno, W.D. Horrocks Jr., R.J. Zauhar, Biochemistry 31 (1992) 7016.
[24] J. Bruno, W.D. Horrocks Jr., K. Bechingham, Biophys. Chem. 63 (1996) 1.
[25] E. Pidcock, G.R. Moore, J. Biol. Inorg. Chem. 6 (2001) 479.
[26] Z.J. Wang, L.X. Ren, Y.Q. Zhao, G.T. Li, A.H. Liang, B.S. Yang, Spectrochim, Acta Part A 66 (2007) 1323.
[27] C.N. Pace, F. Vajdos, L. Fee, G. Grimsley, T. Gray, Protein Sci. 4 (1995) 2411.
[28] J. Hu, X. Jia, Q. Li, X.D. Yang, K. Wang, Biochemistry 43 (2004) 2688.
[29] S.J. Dong, G.L. Che, Y.W. Xie, Chemically Modified Electrodes, Chinese Science Press, Beijing, China, 1995.
[30] S. Richard, W. Nicholson, S. Irving, Anal. Chem. 36 (1964) 706.
[31] S.F. Guo, Q. Zhou, T.H. Lu, X.L. Ding, X.H. Huang, Spectrochim. Acta Part A 27 (2008) 818.
[32] L.J.C. Jeuken, F.A. Armstrong, J. Phys. Chem. B 105 (2001) 5271.
[33] E. Toth, L. Burai, A.E. Merbach, Coordin. Chem. Rev. 216–217 (2001) 363.
[34] R.H. Kretsinger, C.E. Kockolds, J. Biol. Chem. 248 (1973) 3313.
[35] A.C.R. da Silva, F.C. Reinach, Trends Biochem. Sci. 16 (1991) 53.

[36] J.J. Falke, S.K. Drake, A.L. Hazard, O.B. Peersen, Q. Rev. Biophys. 27 (1994) 219.
[37] M.S. Cates, M.B. Berry, E.L. Ho, Q. Li, J.D. Potter, G.N. Phillips, J. Struct. 7 (1999) 1269.
[38] Z.J. Wang, Y.Q. Zhao, L.X. Ren, G.T. Li, A.H. Liang, B.S. Yang, J. Photochem. Photobiol. A: Chem. 186 (2007) 178.
[39] W.D. Horrocks Jr., Method Enzymol. 226 (1993) 495.
[40] M. Minunni, M. Mascini, G.G. Guilbault, B. Hock, Anal. Lett. 28 (1995) 749.
[41] Y.B. He, H.Q. Luo, N.B. Li, Biosens. Bioelectron. 22 (2007) 2952.
[42] Y. Liu, X. Yu, R. Zhao, D.H. Shangguan, Z. Bo, G. Liu, Biosens. Bioelectron. 18 (2003) 1419.